Breast Imaging Using Transmission Ultrasound: Reconstructing Tissue Parameters of Sound Speed and Attenuation

Cuiping Li
Karmanos Cancer Institute
4100 John R. Street
Detroit, MI 48201, USA
lic@karmanos.org

Neb Duric
Karmanos Cancer Institute
4100 John R. Street
Detroit, MI 48201, USA
duric@karmanos.org

Lianjie Huang
Los Alamos National Laboratory, MS D443
Los Alamos, NM 87545, USA
ljh@lanl.gov

Abstract

Multiple tissue parameters are useful for early breast cancer detection and diagnosis. Ultrasound tomography is a new, important imaging modality for our Computerized Ultrasound Risk Evaluation (CURE) prototype, which employs a ring transducer array to scan the whole breast in a water tank. We use our bent-ray time-of-flight ultrasound tomography to reconstruct sound speeds of breasts with different densities. In addition, we develop an ultrasound attenuation reconstruction method based on complex-signal energy ratios. We apply our reconstruction techniques to in vitro and in vivo breast data acquired using the CURE device. Our reconstruction results demonstrate that CURE has great potential to reliably measure multiple mass characteristics by combining sound-speed, attenuation and reflection images.

1. Introduction

A great deal of progress has been made on the use of ultrasound transmissions for early detection and diagnosis of breast cancer [1-4]. In contrast to backscattering, transmission ultrasound has the potential to yield accurate, quantitative sound-speed and attenuation images. A clinical ultrasound scanner with a ring array has been designed and built at Karmanos Cancer Institute (KCI) for breast cancer detection and diagnosis. It is called the Computed Ultrasound Risk Evaluation (CURE). It can record both transmitted and reflected ultrasound signals. A robust ultrasound tomography algorithm is needed to obtain high-resolution reconstructed images. Combining sound-speed and attenuation images with reflection images has the potential to differentiate benign masses from cancerous masses, and can improve the diagnostic capability and clinical utility of CURE. In addition, it has been shown that the sound speed of the breast correlates well with the tissue density. Therefore, sound-speed imaging can be used to accurately trace the glandular tissue of the breast for estimate breast-cancer risk [5].

In this paper, we employ an iterative regularized refraction tomography algorithm to reconstruct sound-speed and attenuation parameters of the breast. In our time-of-flight transmission tomography method, we define a new regularization term to normalize the ray coverage at different model cells, and account for ray bending effects during reconstruction. Our attenuation tomography method uses complex signal energy ratios for reconstruction. It calculates the total energy of an ultrasound signal using the amplitude envelope of the corresponding analytic signal (a complex signal). The amplitude envelope is selected because of its natural separation from signal phase and frequency information, and its insensitivity to small phase shifts. Since the average amplitude envelope is phase and frequency independent, it is more stable in terms of susceptibility to noise contamination compared to the real signal (real part of the analytic signal).

We apply our tomography techniques to an anthropomorphic breast phantom and more than 180 patients' data acquired using CURE. In this paper, we present examples of sound-speed, attenuation images, and the fused image of sound-speed, attenuation and reflection images. Our results imply that CURE has great potential in clinical applications for breast cancer imaging.

2. CURE device and data collection

The CURE device, or the Computerized Ultrasound Risk Evaluation, was developed and built at the Karmanos Cancer Institute (KCI), Wayne State University, Detroit, MI. This clinical prototype has been integrated into the routine patient flow of the Walt Comprehensive Breast Center located at the KCI.

978-0-7695-3118-2/08 $25.00 © 2008 IEEE
DOI 10.1109/BMEI.2008.303

A brief overview of CURE is given here. For details, please refer to [4].

CURE is capable of recording all ultrasound wavefields (including reflected, transmitted, and diffracted ultrasonic signals from the breast tissue) that can be used to reconstruct images of acoustic properties. Figure 1(a) is a schematic representation of the transducer ring. Figure 1(b) illustrates scattering of ultrasound emitted from a transducer element and received by all transducer elements along the ring. There are a total of 256 elements along a 20-cm diameter ring array. Each element can emit and receive ultrasound waves with a central frequency of 1.5 MHz. During the scan, the ring array is immersed into a water tank, and encircles the breast. The signals are recorded at a sampling rate of 6.25 MHz. The whole breast is scanned slice by slice, and the scanned slice data are recorded by a computer for data processing afterwards. A motorized gantry is used to translate the ring along the vertical direction, starting from the chest wall to the nipple. One complete scan takes about 1 minute, and acquires approximately 60-80 slices of data per patient.

Our patient recruitment taps into the standard patient flow of the KCI's Alexander J. Walt Breast Center. The CURE ultrasound exam is performed after mammography and standard ultrasound (US) exams, but before the US guided biopsy.

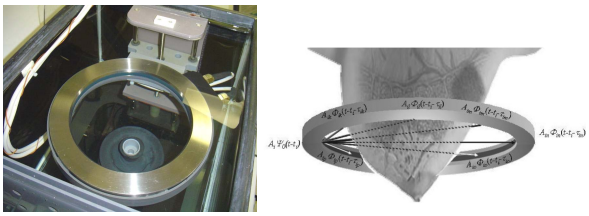

(a) (b)

Figure 1. Clinical prototype of the CURE device. (a) Close-up of the imaging tank showing the transducer ring affixed to a mechanical arm that moves the ring vertically while imaging the entire breast volume; (b) A schematic representation of the CURE ring transducer (From [4]).

3. Ultrasound transmission tomography

3.1 Input data for sound-speed tomography

We have recently developed an automatic time-of-flight (TOF) picker based on Akaike Information Criteria [6]. We use this method to pick TOFs of transmitted ultrasound signals for our bent-ray sound-speed tomography.

3.2 Input data for attenuation tomography

We use the complex signal energy method to generate data for ultrasound attenuation tomography. This method requires localization of the first arrival pulse for each transmission waveform.

A real waveform $y(t)$ can be represented by its amplitude envelope $a(t)$ and phase $\theta(t)$:

$$y(t) = a(t)\cos\theta(t). \quad (1)$$

The corresponding quadrature waveform is

$$y^*(t) = a(t)\sin\theta(t) = -H(y(t)), \quad (2)$$

where $H(y(t))$ is the Hilbert transform of $y(t)$. The analytic waveform $z(t)$ is then give by

$$z(t) = y(t) + iy^*(t). \quad (3)$$

The amplitude envelope is calculated using [7]

$$a(t) = \sqrt{y(t)^2 + y^*(t)^2}. \quad (4)$$

To isolate the first arrival pulse, the beginning of the pulse t_1 is obtained by the pulse's TOF pick. The end of the pulse t_2 is determined by taking the time difference between the start of the pulse and the first envelope peak, then multiplying by a factor [8].

Ultrasound data are acquired right before the breast is immersed into the water tank. Is is called "water data." The signal energy of an analytic waveform of a first-arrival pulse is calculated using eq. (4). The complex energy ratio between a breast ultrasound signal and that propagating through water is used for attenuation tomography. Therefore, the estimated attenuation parameters are relative to water.

The total complex energy for water data is

$$E_W = \int_{t_1}^{t_2} |W(t)|^2 \, dt, \quad (5)$$

Where W is the amplitude envelope of water data. Similarly, the total complex energy for breast data is

$$E_B = \int_{t_1'}^{t_2'} |R(t)|^2 \, dt, \quad (6)$$

where t_1', t_2', R are the same parameters as in eq. (5) but for the breast data. The effective attenuation is

$$C = \int_{ray} a_0 dl = \log_{10}(\frac{E_w}{E_B}) / f_n, \quad (7)$$

where f_n is the Nyquist frequency, which is 3.125 MHz for CURE data.

3.3 Tomography method

Based on the Fermat's principle and Snell's law, ultrasound rays in inhomogeneous media (such as breast tissue) are not straight. In this study, a bent-ray ultrasound tomography algorithm with a new regularization term is used. During each iteration step of sound-speed reconstruction, both the forward problem and the inverse problem are solved, and the sound-speed model is updated for the successive iterations.

In the forward problem, calculated TOFs are calculated by solving the eikonal equation

$$\begin{aligned}(\nabla E)^2 &= (\partial T/\partial x)^2 + (\partial T/\partial y)^2 \\ &= (1/v)^2 = (s_x^2 + s_y^2)\end{aligned}, \quad (8)$$

where T is the travel-time, v is the sound-speed, and (s_x, s_y) is a slowness vector of ultrasound wave. The slowness is the inverse of sound speed. In eq. (8), $E = const.$ describes the 'wavefronts', and 'rays' are defined as the orthogonal trajectories of these wavefronts. Equation (8) is solved using Klimes' grid travel-time tracing technique [9], which has been proven to be both accurate and fast. An ultrasound ray is traced by backprojection from a receiver to a transmitter.

Let Δt_i be the difference between the i^{th} picked TOF for a recorded ultrasound signal and the correspoinding i^{th} calculated TOF for a sound-speed model at a given iteration step. The inverse problem is

$$\sum_j^M l_{ij} \Delta s_j = \Delta t_i, \quad (9)$$

where Δs_j is the slowness perturbation for the j^{th} grid cell that needs to be inverted, and l_{ij} is the ray length of the i^{th} ray within the j^{th} cell. Equation (9) can be expressed as a matrix form

$$L\delta S = \delta T. \quad (10)$$

This is a nonlinear inverse problem due to ray bending. The following regularized tomography inversion algorithm is used to solve for δS:

$$\delta S = (L^* C_d^{-1} L + \alpha C_{x_0}^{-1} + \beta I)^{-1} L^* \delta T, \quad (11)$$

where C_d^{-1} is the inverse data covariance matrix, $C_{x_0}^{-1}$ is the inverse a priori model covariance matrix, α and β are regularization parameters that balance the smoothness of the inverted results and the fit to the data. In this paper, a identity matrix I is used for C_d^{-1}. The regularization term $C_{x_0}^{-1}$ is given by

$$C_{x_0}^{-1} = \sqrt{diag(L^* L)}, \quad (12)$$

whose diagonal element $\sum_{i=1}^{m} l_{ij}^2$ is the total ray length within the j^{th} grid cell that renormalizes the inverse problem for unequal ray coverage. The smoothing term (βI) in eq. (11) is to compensate those grid cells without any ray coverage.

Paige and Saunders' LSQR method [10] is used to iteratively solve the nonlinear problem in eq. (11) for δS, starting with a homogeneous sound-speed model. After each iteration step, an updated model is obtained by adding the solution δS to the initial model. Rays are traced on the updated model to obtain updated TOF data. The iteration continues until the solutions converge.

For attenuation tomography, after the effective attenuation $C = \int_{ray} a_0 dl$ is obtained, the attenuation parameter a_0 is reconstructed by solving the discretized inverse problem

$$\sum_j l_{ij} a_{0j} = C_i, \quad (13)$$

where a_{0j} is the attenuation parameter for the j^{th} model cell, and l_{ij} is the the ray length of the i^{th} ray within the j^{th} cell. We first use TOFs of transmission ultrasound signals to reconstruct the breast sound-speed distribution, then trace bent-ray paths and use eq. (13) to reconstruct attenuation parameter a_0.

4. Results

We apply our ultrasound tomography algorithm to the breast phantom data acquired using CURE. A phantom's cross-sectional CT scan, reconstructed sound-speed and attenuation images are shown in Figs. 2(a)-(c), respectively. Comparison of the reconstructed sound-speeds to their known sound-speeds shows that our sound-speed reconstruction has an overall accuracy of approximate 5 *m/s*. However, for small inclusions, the differences tend to be bigger (15 *m/s* for 6 mm

mass and 19 *m/s* for 9 mm mass, which are labeled as 2 and 4 in Fig. 2(a), respectively).

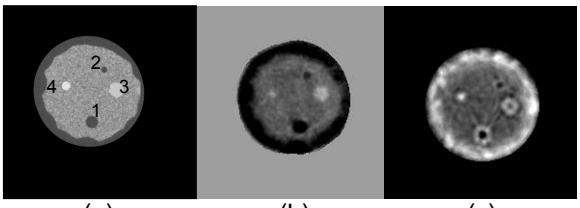

Figure 2. Tomography images of *in vitro* ultrasound breast data acquired using CURE. (a) X-ray CT scan of the breast phantom. (b) Sound-speed reconstruction. (c) Attenuation reconstruction. In (a), (b) and (c), all x and y axes span 200 mm in length.

We have applied our sound-speed and attenuation tomography method to more than 180 *in vivo* ultrasound breast datasets acquired using CURE. The clinical protocol is designed to include a sample of patients with a wide variety of breast types, ranging from fatty to dense on the BI-RADS categories 1-4. Figure 3 presents examples of our sound-speed and attenuation tomograms for different breast types with and without masses. In Fig. 3, the left panel of each row is a sound-speed tomogram, and the right panel is the corresponding attenuation tomogram. Figure 3(a) is a fatty breast with a small mass at 12 o'clock. It is 5.7 mm in size as described in the clinical US report. Figure 3(b) shows the sound-speed distribution and attenuation for a breast with scattered fibroglandular tissue, which has a poorly differentiated infiltrating ductal carcinoma at 8:00 o'clock (as indicated by the clinical mammogram report). The breast in Fig. 3(c) is composed of heterogeneous dense fibroglandular tissue with an invasive, poorly differentiated carcinoma at 2:00 o'clock. The breast in Fig. 3(d) is a very dense breast with benign breast tissue.

Because the resolution limit of our tomography algorithm is approximately 3 wavelengths (or 3 mm for CURE), we do not expect our reconstructions to be sensitive to the fibrous structure of the breast. However, the images in Fig. 3 show that the fatty and glandular tissues are well characterized.

Statistically, the malignant masses have elevated values of sound-speed and attenuation parameters relative to the surrounding tissue. Moreover, the architectural distortion in the tumor region of a reflection image is another indicator of cancer [11]. Therefore, fusing sound-speed, attenuation and reflection images together can visually enhance the breast mass. Figure 4 (left) is such a fused image, which shows a local enhancement of sound-speed and attenuation in the tumor region. To obtain a visually better fused image, the inverted RGB instead of RGB are used, where the sound-speed image is presented as pink (inverted green), attenuation is yellow (inverted blue), and reflection image is greenish blue (inverted red). The legend is shown in the right panel of Fig. 4.

5. Conclusions

We have implemented a bent-ray sound-speed and attenuation tomography algorithm for transmission ultrasound data acquired using a clinical prototype ring transducer array. We have also developed a new method to estimate the effective total attenuation of the breast utilizing a complex signal energy method. *In vitro* applications to a breast phantom and *in vivo* applications to different types of the breasts in the BI-RADS categories of 1-4, have demonstrated that our tomography method can provide a promising tool for breast mass detection. The correlation among sound-speed, attenuation and reflection (three modalities of CURE) can locally enhance breast masses.

Reconstructed breast sound-speed distribution has another potential clinical value. Glide et al [5] studied the correlation between sound-speed and density of the breast and found that dense breasts generally have high sound speeds. Therefore, whole-breast sound-speed can be used as an overall indicator of breast density, which is an important risk factor for breast cancer.

Acknowledgements

The authors wish to thank Lisa Bey-Knight for her help in recruiting patients and data collection. This work was supported through the Karmanos Cancer Institute and through a grant from the Michigan Economic Development Corporation (Grant Number 06-1-P1-0653). L. Huang acknowledges the support of the U.S. DOE Laboratory-Directed Research and Development program at Los Alamos National Laboratory.

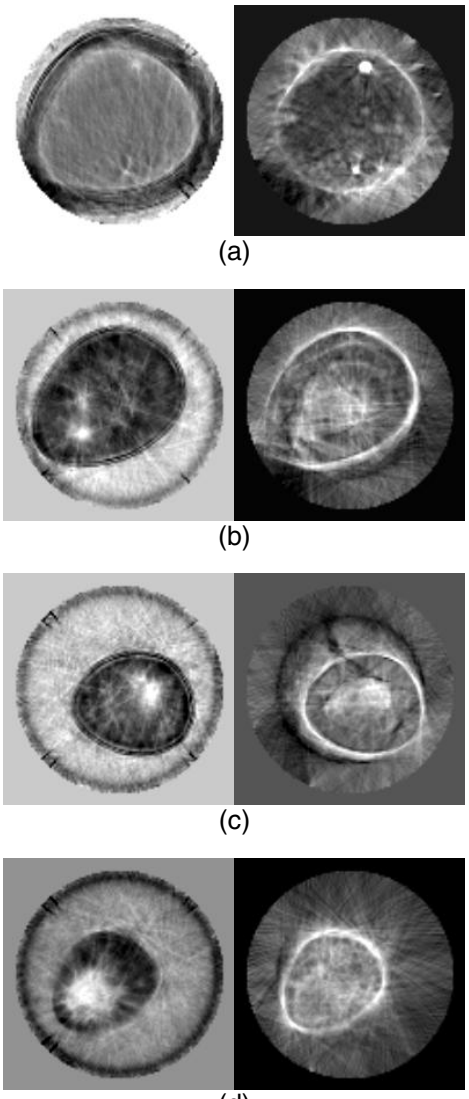

Figure 3. Sound-speed and attenuation reconstructions for breasts of types (a) A fatty breast; (b) A breast with scattered fibroglandular tissue; (c) A breast composed of heterogeneous dense fibroglandular tissue; (b) A dense breast. Left panel: sound-speed. Right panel: attenuation.

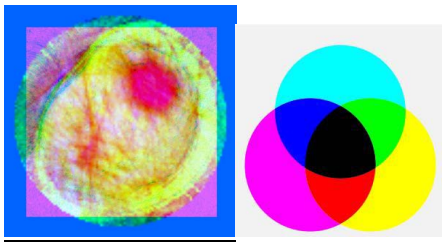

Figure 4. Multimodality CURE imaging. Left: Fused image by superimposing sound-speed (pink), attenuation (yellow) and reflection (greenish blue) images together. Right: Legend.

References

[1] J.F. Greenleaf, A. Johnson, R.C. Bahn, and B. Rajagopalan, "Quantitative cross-sectional imaging of ultrasound parameters." *Ultrasounics Symposium Proceedings,* 1977, pp. 989-995.

[2] P.L. Carson, C.R. Meyer, A.L. Schezinger, and T.V. Oughton, "Breast imagin in coronal planes with simultaneous pulse echo and transmission ultrasound." *Science,* 1981, 214, pp. 1141-1143.

[3] J.F. Greenleaf, J. litalo, and J.J.Gisvold, "Ultrasonic computed tomography for breast examination." *IEEE Engineering in Medicine and Biology,* 1987, pp. 27-32.

[4] N. Duric, P. Littrup, L. Poulo, A. Babkin, R. Pevzner, E. Holsapple, O. Rama, and C. Glide, "Detection of breast cancer with ultrasound tomography: First results with the Computed Ultrasound Risk Evaluation (CURE) prototype." Medical Physics, 2007, 34, pp. 773-785.

[5] C. Glide, N. Duric, and P. Littrup, "Novel approach to evaluating breast density utilizing ultrasound tomography." *Medical Physics*, 2007, 34, pp. 744-753.

[6] C. Li, L. Huang, N. Duric, H. Zhang, and C. Rowe, "An improved automatic time-of-flight picker for medical ultrasound tomography." Submitted to Ultrasounics.

[7] M.T. Taner, F. Koehler, and R.E. Sheriff, "Complex seismic trace analysis." *Geophysics*, 1979, 44, pp.1041-1063.

[8] M.P. Matheney, and R.L. Nowack, "Seismic attenuation values obtained from instantaneous-frequency matching and spectral ratios," *Geophys. J. Int*., 1995, 123, pp. 1-15.

[9] L. Klimes, "Grid Travel-time Tracing: Second-order Method for the first Arrivals in Smooth Media." *Pageoph*, 1996, 148, pp. 539-563.

[10] C.C. Paige, and M.A. Saunder, "LSQR: An Algorithm for Sparse Linear Equations and Sparse Least Squares." *ACM Transactions on Mathematical Software,* 1982, 8, pp. 43-71.

[11] A.T. Stavros, D. Thickman, C.L. Rapp, M.A. Dennis, S.H. Parker, and G.A. Sisney, "Solid breast nodules: use of sonography to distinguish between benign and maligmant lesions." *Radiology*, 1995, 196, pp. 123-134.